LANGRANGIAN PARTICLE MOTIONS IN SUPEFLUID HELIUM AND THEIR INTERACTION WITH QUANTUM VORTICES

Pasan Sanjeeva
Department of Energy Engineering
Nagoya University
Chikusa Ward, Nagoya, Aichi 464-8601, Japan
sanjeeva.pasan@gmail.com

Yoshiyuki Tsuji
Department of Energy Engineering
Nagoya University
Chikusa Ward, Nagoya, Aichi 464-8601, Japan
c42406a@nucc.cc.nagoya-u.ac.jp

ABSTRACT

Analyzing particle-vortex interaction is essential to interpret the results from particle-laden experiments and reveal flow physics of thermal counterflow of superfluid He II. The two events, trapping and de-trapping of particles on quantized vortices, were experimentally analyzed by using two-dimensional Lagrangian trajectories of particles. A comparison of the ensemble-averaged particle kinetic energy increments between trapping and de-trapping suggests that the two processes are governed by distinct physical mechanisms, with de-trapping associated with a greater loss of particle kinetic energy than trapping.

INTRODUCTION

Quantum turbulence in thermal counterflow of superfluid He has become an important topic in fundamental science and cryogenic applications. The counterflow was first modelled by Landau, by considering an interpenetrating mixture of two fluid components called normal fluid and superfluid (Landau, 1941). In 1946, Lars Onsager had suggested the idea of quantized circulation in superfluid He. The vortex lines with quantized circulation in superfluid was first introduced by Feynman (Donnely, 1991). Quantized vortices were first visualized through images of micrometer-sized particles introduced into the flow, which became trapped on the vortices (Bewley et al., 2006). By employing such particle-tracking techniques, previous studies of thermal counterflow have reported a bimodal distribution of the velocity component in the normal-flow direction, attributed to particles trapped within the vortex tangle (Paoletti et al., 2008). In addition, another study has revealed frequent interactions between particles and quantized vortices by analyzing individual particle trajectories (Švancara et al., 2021). These particle–vortex interactions significantly affect particle motion and the resulting statistical properties. Therefore, for a proper interpretation of particle dynamics and the underlying flow physics in particle-laden experiments, it is essential to investigate particle–vortex interactions, particularly trapping (TR) and de-trapping (DTR) processes.

Furthermore, numerical simulations of Gross-Pitaevskii equation have focused on mechanism of particle trapping by single straight vortex line, and Kelvin waves (KW) along the vortex line which are induced by the interaction (Giuriato and Krstulovic, 2019). Another analysis has shown KW generation during particle trapping and de-trapping events, and vortex stretching (i.e. increasing the length of vortex lines) during de-trapping (Kivotides et al., 2008). Although these numerical studies further emphasize the influence of particle trapping and de-trapping on particle and vortex dynamics, they are limited by neglecting normal fluid flow and by considering only a single particle interacting with a single straight vortex line. This situation motivated us to analyse TR and DTR events through a vortex tangle in thermal counterflow experiment, where both normal fluid flow and superfluid flow are present. Therefore, TR and DTR events were extracted from Lagrangian trajectories of particles and ensemble-average of particle kinetic energy increments for the two events was compared by following Xu et al. (2014) where particle's specific kinetic energy (*KE*) was adopted in classical turbulence through flight crash events in which particles gain *KE* gradually and then suddenly lose it.

EXPERIMENTAL FACILITY

As shown in Figure 1, a vertical channel with a square cross-section was equipped with a heater plate mounted at its bottom surface. The channel was fully immersed in liquid helium within a cryostat to generate thermal counterflow and it was 260 mm in length with a cross section of 20 mm×20 mm. A laser sheet with a thickness of 1 mm was used to illuminate the field of view at center of the duct. A hydrogen–helium gas mixture (H : He = 1 : 40) was introduced into the channel to generate solid hydrogen particles. The present measurements were conducted at a temperature of 2.0 K, with a maintained heat flux of 800 W/m² applied from the heater plate. Under thermal counterflow conditions, the normal fluid flows vertically upward, while the superfluid moves downward, ensuring zero net mass flux across the channel cross-section. These opposing motions are reflected in the bimodal probability density function of the particle velocity component along the heat flux direction (Paoletti et al. 2008). A high-speed camera operating at 250 frames per second (fps) was used to capture images of solid hydrogen particles,

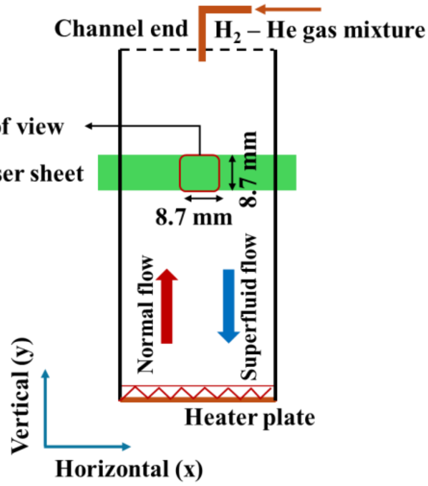

Figure 1. The channel with a heater at the bottom. The field of view is 8.7 mm × 8.7 mm. In the thermal counterflow, red arrow shows normal flow and blue arrow is for superfluid flow. Vertical (y) and horizontal (x) directions of the flow are as shown by the arrows.

Figure 2. A sample image of small particles taken during experiment (White colour dots are small particles).

as shown in Figure 2. Further details of the experimental setup can be found in Chen et al. (2022).

DATA ANALYSIS

The images are used to generate two-dimensional Lagrangian particle trajectories from an in-house PTV code. Small tracer particles with an average diameter of 12 μm are selected from the overall size distribution, assuming a log-normal distribution following Kubo and Tsuji (2019), and their trajectories are subsequently constructed. The instantaneous velocity vector along particle trajectory, $\boldsymbol{U}$ is calculated using central differencing method as,

$$\boldsymbol{U} = \frac{\boldsymbol{x_p}(t+\tau) - \boldsymbol{x_p}(t-\tau)}{2\tau}, \quad (1)$$

Where τ denotes time lag between successive position measurements and $\boldsymbol{x_p}$ denotes particle position vector along trajectory.

Instantaneous fluctuating velocity vector, $\boldsymbol{u'}$ along Lagrangian particle trajectories is calculated as,

$$\boldsymbol{u'} = \boldsymbol{U} - \langle \boldsymbol{U} \rangle, \quad (2)$$

Where $\boldsymbol{u'} = u'_x\boldsymbol{i} + u'_y\boldsymbol{j}$, and u'_x and u'_y denote the fluctuating velocity components in x and y directions, respectively. $\langle \boldsymbol{U} \rangle$ is the average velocity determined by all particle trajectories, and it represents the bulk flow of particles. $\boldsymbol{u'}$ can be interpreted as the particle velocity observed in a reference frame moving with the average velocity $\langle \boldsymbol{U} \rangle$. Therefore, this analysis is performed relative to this reference frame.

In this analysis, specific particle kinetic energy (*KE*) and its increments (*W(τ)*) along Lagrangian particle trajectories are the fundamental physical quantities. These quantities are calculated as,

$$KE = (1/2)(\boldsymbol{u'} \cdot \boldsymbol{u'}), \quad (3)$$

$$W(\tau) = KE(t+\tau) - KE(t). \quad (4)$$

where $\boldsymbol{u'}$ is the instantaneous fluctuating velocity vector as defined by Equation 2. $\tau = b\tau_0$ (b = 1,2,3). τ_0 is the smallest time lag (4 ms) associated with 250 fps of the experiment. b is a parameter used to represent the three different time-lag values. To examine particle–vortex interactions across different flow scales, modified trajectories are generated for each time lag (τ) by removing particle positions from the original trajectories obtained at the smallest time lag, following the approach in La Mantia and Skrbek (2014). The number of time lags considered in this analysis is constrained by the available experimental data. The particle fluctuating velocity ($\boldsymbol{u'}$), kinetic energy (*KE*), and its increment (*W(τ)*) are then evaluated along the trajectories constructed for each time lag.

Figure 3 shows a sample particle trajectory with trapping (Circle A) and de-trapping (Circle B). Points indicated by S and E represent starting and end positions of the trajectory respectively. The arrows show the direction of particle motion. We infer that trapping and de-trapping processes occur in these turning regions where particles change their vertical motion (see regions A and B in Figure 3) in opposite direction since the two fluid components in the counterflow move in opposite direction. Note that the trapping and de-trapping events are not defined as occurring at a single instant. Rather, they are considered as processes that evolve over time in these turning regions. Also, it is difficult to distinguish a unique instant at which a particle becomes trapped or de-trapped on the discrete particle trajectories. A local average of fluctuating vertical velocity component (u'_y), based on neighboring values, is computed at each position along trajectory. This average vertical velocity is then used to identify turning points during TR and DTR, as it reduces fluctuations and detects turning points robustly. Note that the sign changes from positive to negative for the turning points of TR and vice versa for DTR; positive indicates upward motion and negative indicates downward motion.

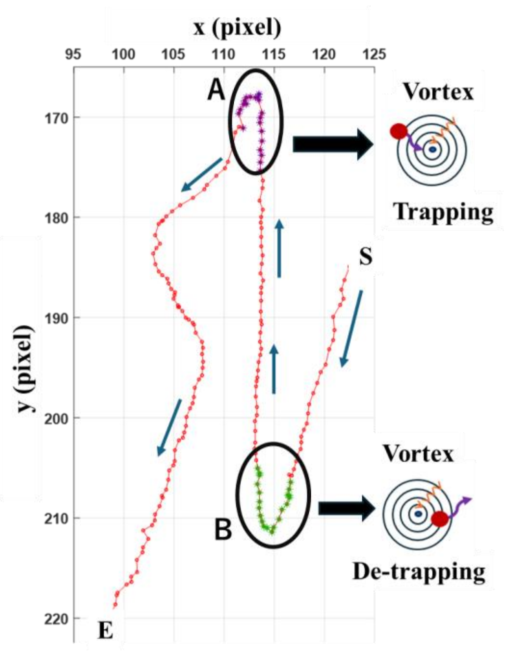

Figure 3. A sample trajectory with a trapping (Circle A) and a de-trapping (Circle B) events. S and E denote starting and end positions of the trajectory.

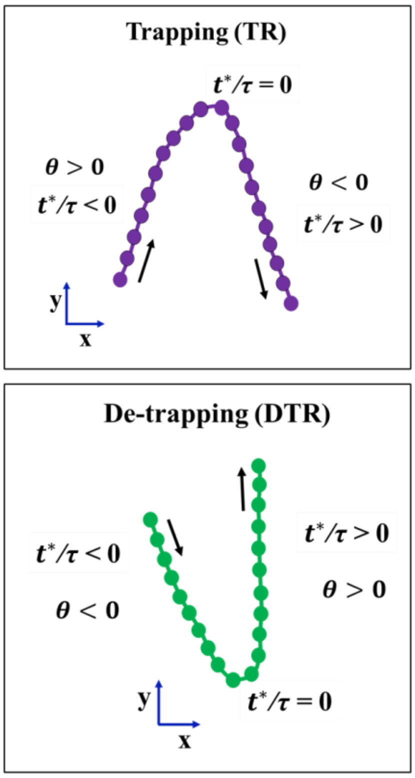

Figure 4. Illustration of TR and DTR events. $t^*/\tau = 0$, denotes turning point of TR and DTR events. $t^*/\tau < 0$ is before turning point and $t^*/\tau > 0$ is after turning point. Black arrows show moving direction of particles in TR and DTR events.

The method based solely on the locally averaged vertical velocity is insufficient to precisely identify TR and DTR events. Therefore, the orientation angle (θ) of the instantaneous fluctuating velocity vector ($\boldsymbol{u'}$) is also computed as,

$$\theta = tan^{-1}\left(\frac{u'_y}{u'_x}\right). \tag{5}$$

Here, u'_x and u'_y indicate velocity components of the fluctuating velocity ($\boldsymbol{u'}$) in x and y direction respectively. θ has the range of $-\pi < \theta < \pi$. By examining particle trajectories while varying the range of θ values, an appropriate value range for θ is chosen to extract distinct TR and DTR events.

Since the extracted TR and DTR events occur at different times in the experiment, a virtual time t^* is assigned to each event, with $t^* = 0$ defined at the turning point as a reference. The virtual time t^* is then normalized by the time lag τ, which represents the interval between two consecutive positions along a particle trajectory. Thus, $t^*/\tau = 0$ corresponds to the turning point, $t^*/\tau < 0$ indicates times before the turning point, and $t^*/\tau > 0$ indicates times after the turning point, as shown in Figure 4. This normalization enables all extracted events (TR or DTR) to be mapped onto a common dimensionless time axis, allowing the ensemble-averaged particle kinetic energy increments to be computed separately for TR and DTR events and facilitating direct comparison of their patterns.

For each time lag (τ), hundreds of TR and DTR events are separately extracted from the particle trajectories. To gain insight into particle kinetic energy variation in these extracted TR and DTR events, ensemble-average of $W(\tau)$ at each normalized time t^*/τ for a given time lag of τ is computed respectively as,

$$\langle W(t^*/\tau, \tau)\rangle = \frac{1}{N}\sum_{k=1}^{N} W_k(t^*/\tau, \tau). \tag{6}$$

$W_k(t^*/\tau, \tau)$ is kinetic energy increment at t^*/τ with time lag of τ for k-th event, respectively. N is the number of extracted TR or DTR events. The conditional ensemble-average is then computed as a function of t^*/τ for TR and DTR events separately and plotted together for direct comparison of their patterns.

RESULTS AND DISCUSSION

In this section, we present selected results accompanied by a brief discussion. The conditional ensemble-average of *W(τ)* against t^*/τ for trapping and de-trapping have been plotted on Figure 5 at different time lags (τ) respectively. The plot at different time lags (τ) is shifted upwards for clarity. The red dashed lines in Figure 5 show zero reference of $\langle W(t^*/\tau, \tau)\rangle$ for each time lag (τ) and shifted upwards by the same amount.

As shown in Figure 5, the kinetic energy of the particle decreases noticeably during de-trapping (DTR) compared with trapping (TR), as more negative values of $\langle W(t^*/\tau, \tau)\rangle$ are observed in the DTR process. This suggests that particles undergoing de-trapping may experience more intense interactions than during trapping.

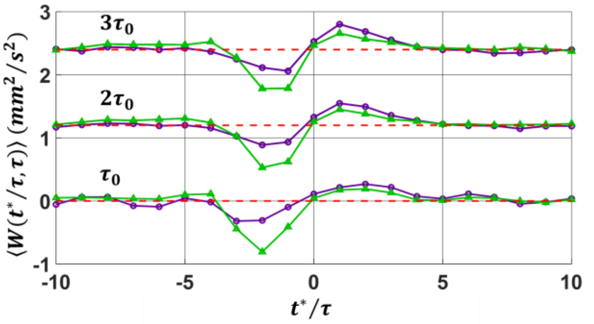

Figure 5. $\langle W(t^*/\tau, \tau)\rangle$ against t^*/τ for TR and DTR (● – TR, ▲- DTR). $\tau = \tau_0, 2\tau_0, 3\tau_0$ ($\tau_0 = 4ms$) and $t^*/\tau = 0$ at the turning point of TR and DTR.

One possible explanation is that, during trapping, a particle moving upward with the normal fluid interacts primarily with a single quantum vortex line. In contrast, during its subsequent downward motion within the vortex tangle, multiple vortex lines may reconnect to the particle's outer surface. As a result, during de-trapping, the particle is likely to interact simultaneously with several vortex lines. To assess the plausibility of this scenario, the intervortex spacing was roughly estimated from previous studies (Adachi et al., 2010; Babuin et al., 2012; Verga and Skrbek, 2018), yielding values of approximately 300 µm at 300 W/m² and 100 µm at 800 W/m². The particle sizes considered in the present analysis are smaller than these mean intervortex distances for both heat flux conditions. However, at 800 W/m², the intervortex spacing is only a few times larger than the particle size, whereas at 300 W/m², the difference is considerably greater.

In addition, particle trajectory observations indicate that trapped particles can travel with the superfluid over distances exceeding the mean intervortex spacing until its subsequent de-trapping event. This suggests that interactions between a trapped particle and multiple vortex lines may have a possibility at a heat flux of 800 W/m² than at 300 W/m². Furthermore, not only the presence of multiple vortex lines but also the drag force exerted by the surrounding normal fluid may contribute to the stronger interactions observed during de-trapping (DTR). Nevertheless, further detailed investigations are necessary to clarify the underlying mechanisms.

CONCLUSION

In summary, the motion of small particles during trapping (TR) and de-trapping (DTR) events in the thermal counterflow of superfluid He II was investigated. These TR and DTR events were identified from two-dimensional Lagrangian particle trajectories, and they were analyzed using the particles' specific kinetic energy (*KE*). Comparison of the conditional ensemble-average of particle kinetic energy increments between TR and DTR suggests that the two events involve different mechanisms in thermal counterflow across the time scales of τ_0, $2\tau_0$, $3\tau_0$. Further investigations are required to understand the mechanism of trapping and de-trapping events in a vortex tangle in the thermal counterflows where both normal flow and superfluid flow are present, and to examine the time lag-invariant behavior over a wide range of flow scales.

ACKNOWLEDGEMENT

The author (Pasan Sanjeeva) gratefully acknowledges the scholarship grant provided by the Yoshida Scholarship Foundation, Tokyo. The authors also wish to express our gratitude to Mr. T. Maruyama for his assistance during the measurements. This work was partially supported by JSPS KAKENHI Grant Numbers JP 19H00747 and JP25K01154.

REFERENCES

Adachi A., Fujiyama S., Tsubota M., 2010, "Steady state thermal counterflow turbulence: Simulation of vortex filaments using the full Biot-Savart law", *Phys. Rev. B,* Vol. 81.

Babuin S., Stammeir M., Varga E., Rotter M., and Skrbek L., 2012, "Quantum turbulence of bellows-driven ^{4}He superflow: Steady state", *Phys. Rev. B*, Vol. 86.

Bewley, G. P., Lathrop, D. P., and Sreenivasan, K. R., 2006, "Visualization of Quantized Vortices", *Nature*, Vol. 441.

Chen, L., Maruyama, T., and Tsuji, Y., 2022, "Statistical Properties of Lagrangian Trajectories of Small Particles in Superfluid 4He", *J. Low Temp. Phys*., Vol.208.

Donnely, R. J., 1991, "Quantized Vortices in Helium II", Cambridge University Press.

Giuriato, U., and Krstulovic, G., 2019, "Interaction Between Active Particles and Quantum Vortices Leading to Kelvin Wave Generation", *Scientific Reports*, Vol.9.

Kivotides, D., Barenghi, C. F., and Sergeev, Y. A., 2008, "Interaction Between Particles and Quantized Vortices in Superfluid Helium", *Phys. Rev. B*, Vol. 77.

Kubo, W., and Tsuji, Y., 2019, "Statistical Properties of Small Particle Trajectories in a Fully Developed Turbulent State in He-II", *J. Low Temp. Phys*., Vol. 196.

Landau L, (1941). Theory of the Superfluidity of Helium II. *Physical Review*, Vol. 60.

La Mantia, M., and Skrbek, L., 2014, "Quantum, or Classical Turbulence?", *The Frontiers of Physics*, Vol. 105.

Paoletti, M. S., Fiorito, R. B., Sreenivasan, K. R., and Lathrop, D. P., 2008, "Visualization of Superfluid Helium Flow", *J. Phys. Soc. Jpn.*, Vol.77.

Švancara, P., Duda, D., Hrubcová, P., Rotter, M., Skrbek, L., La Mantia, M., Durozoy, E., Diribarne, P., Rousset, B., Bourgoin, M., and Gibert, M., 2021, "Ubiquity of Particle-Vortex Interactions in Turbulent Counterflow of Superfluid Helium", *J. Fluid Mech.*, Vol. 911.

Varga E. and Skrbek L., 2018, "Dynamics of the density of quantized vortex lines in counterflow turbulence: Experimental investigation", *Phys. Rev. B*, Vol. 97.

Xu, H., Pimir, A., Falkovich, G., Bodenschatz, E., Shats, M., Xia, H., Francois, N., and Boffetta, G., 2014, "Flight-Crash Events in Turbulence", *PNAS*, Vol. 111.